J Solid State Electrochem (2008) 12:583–589
DOI 10.1007/s10008-007-0407-0

ORIGINAL PAPER

Ammonia oxidation on electrodeposited Pt–Ir alloys

E. Moran · C. Cattaneo · H. Mishima · B. A. López de Mishima · S. P. Silvetti · J. L. Rodriguez · E. Pastor

Received: 26 September 2006 / Revised: 7 June 2007 / Accepted: 8 August 2007 / Published online: 18 September 2007
© Springer-Verlag 2007

Abstract Ammonia electro-oxidation on Pt–Ir alloys has been studied applying cyclic voltammetry and differential electrochemical mass spectrometry (DEMS), and the results were compared with pure Pt. Bimetallic alloys were prepared by electrodeposition and characterized using X-ray diffractometry (XRD) and Auger spectroscopy, before and after oxidation of ammonia. Pt/Ir atomic composition was 70:30 obtained from 1:1 solutions. Substitution alloys were established where Ir atoms replace Pt positions in the face-centered cubic structure. Preferential crystal orientations were detected in the electrodeposits with the development of a crystallographic texture. DEMS showed that N_2 is the main product during ammonia oxidation for both Pt and Pt–Ir, but the formation of nitrogen oxides is observed for $E>0.8$ V_{RHE}. The yield of N_2 is higher for the alloy, which also displays lower poisoning of the surface when increasing ammonia concentration. These results confirm Pt–Ir alloys as alternatives to Pt electrodes concerning ammonia oxidation. Finally, it was observed that XRD patterns, as well as texture coefficient values, change after using the electrodeposits for ammonia oxidation, with the less compact planes the more affected ones.

Keywords Pt–Ir electrodeposited alloys · XRD · Auger spectroscopy · Ammonia oxidation Cyclic voltammetry · DEMS

Dedicated to Prof. Dr. Teresa Iwasita on the occasion of her 65th birthday in recognition of her numerous contributions to interfacial electrochemistry.

E. Moran · C. Cattaneo · H. Mishima ·
B. A. López de Mishima (✉)
Instituto de Ciencias Químicas,
F.A.A. Universidad Nacional de Santiago del Estero,
Avda. Belgrano (s) 1912,
4200 Santiago del Estero, Argentina
e-mail: bmishima@unse.edu.ar

S. P. Silvetti
FAMAF, Universidad Nacional de Córdoba,
Ciudad Universitaria,
5000 Córdoba, Argentina

J. L. Rodriguez · E. Pastor
Departamento de Química Física,
Universidad de la Laguna,
C/Astrofísico Francisco Sánchez s/n,
38071 Tenerife, Spain

Introduction

The electrocatalytic oxidation of ammonia in alkaline solutions has become an important topic in environmental electrochemistry, as ammonia is a common and highly toxic component in continental waters because of its use as fertilizer in agriculture. On the other hand, this reaction has received attention in the 1960s and 1970s in the context of possible fuel cell applications: Ammonia can be considered a good candidate for fuel cells under conditions where only N_2 is formed because of the low standard potential of this oxidation reaction, the high theoretical electrical charge density, and the absence of contamination products. Thus, from both an ecological and energetic point of view, the study of the mechanism of the anodic oxidation of ammonia on different metallic and oxide catalysts electrodes has received much attention ([1–4] and reference therein).

The oxidation of ammonia on platinum catalysts can take place electrochemically in alkaline solution (for example, see references [5–9]) or using oxygen as the oxidizing agent [10]. A similar mechanism seems to occur in the electrochemical and liquid-phase oxidation of

ammonia, and in both cases, the selectivity of the reaction is dependent on the presence of oxides at the surface. Thus, the formation of oxides occurs at 0.80 V_{RHE} within the electrochemical environment, and it is avoided in the oxidation with oxygen when the gas supply is diffusion limited. In the absence of oxides, only N_2 is formed, whereas oxygen-containing species like N_2O and NO_2^- are produced if they are present.

The oxidation of ammonia involves the breaking of N–H bonds and the formation of N–N bonds. The most accepted mechanism was suggested by Gerischer and Mauerer [11] for platinized Pt. They considered that the reaction proceeds by a sequence of steps involving the progressive dissociation of ammonia into amine and imine radicals with the formation of molecular nitrogen as the final reaction product:

$$NH_{3(aq)} \rightarrow NH_{3(ads)} \quad (1)$$

$$NH_{3(ads)} \rightleftarrows NH_{2(ads)} + H^+ + e \quad (2)$$

$$NH_{2(ads)} \rightarrow NH_{(ads)} + H^+ + e \quad (3)$$

$$NH_{(ads)} \rightarrow N_{(ads)} + H^+ + e \quad (4)$$

$$NH_{x(ads)} + NH_{y(ads)} \rightarrow N_2 + (x+y)H^+ + (x+y)e \quad (5)$$

where x, y=1 or 2. The authors assumed that the adsorption of ammonia is fast and the surface achieves saturation. $N_{(ads)}$ species blocks the surface whereas $NH_{2(ads)}$ and $NH_{(ads)}$ are the active species, which recombine in reaction 5 to give N_2H_x (x=2–4) adspecies as intermediates, which finally dehydrogenate to form N_2. The recombination of NH_x species is proposed to be the rate-determining step. According to Gerischer and Mauerer [11], the adsorption energy for N_{ads} is too high to enable N_2 formation by recombination of two N adatoms.

This mechanism has been recently analyzed for the different Pt basal planes [9]. It was observed that ammonia oxidation on Pt is a very sensitive process that takes place almost exclusively on (100). The oxidation on the three planes leads to the same gaseous products (N_2, NO, and N_2O) with differences in the yield and the onset potential for these compounds. On Pt(100), a poison that inhibits the formation of N_2 but not that of N_2O is established [9]. In this case, NO is produced at potentials more positive than 0.90 V_{RHE} [9].

Other metals can be also interesting for this oxidation reaction. Studies in the gas phase have shown that noble transition metals (Pt, Pd, Rh, and Ir) are the most active catalysts, whereas the coinage metals (Cu, Ag, and Au) are less active, being Ir the most selective toward the oxidation to N_2 [12–14]. At metal/liquid interfaces, the questions that arise are the possibility that the Gerisher–Mauerer mechanism also applies to other transition and noble metal electrodes and the link between N_2 production and the stability of the adsorbates. With this purpose, de Vooys et al. [15, 16] investigated the role of adsorbates in the electrochemical oxidation of ammonia on Ru, Pd, Rh, Ir, Pt, Cu, Ag, and Au. The authors observed that the activity in the selective oxidation to N_2 is directly related to the nature of the species at the surface: The metal is active if $NH_{x(ads)}$ species are present and deactivates if $N_{(ads)}$ is formed, this process being potential dependent. The trend in the strength of adsorption of $N_{(ads)}$ is Ru>Rh>Pd>Ir>Pt>>Au, Ag, Cu, which corresponds with that for the calculated heat of adsorption of atomic nitrogen, except for the case of Ir. Moreover, for the latter, the $N_{(ads)}$ saturation coverage is lower compared with the other transition metals. Finally, it was concluded that only Pt and Ir combine a good dehydrogenation capacity with a sufficiently low affinity for the formation of $N_{(ads)}$ to lead to a steady-state-production of the active intermediates needed to form N_2 [15].

According with these results, Ir seems to be an alternative to Pt for the ammonia oxidation reaction but, as these authors suggested in de Vooys et al. [15], the bimetallic catalyst would enable a better understanding of the role of absorbates on these processes, especially Pt–Ir alloys, which have been reported to show a higher activity than the individual metals [7, 17]. However, only few investigations on the alloyed electrocatalysts have been performed [18, 19], and this is the aim of the present paper. Thus, ammonia oxidation was studied at Pt–Ir alloys prepared by electrodeposition and compared with Pt.

It is remarkable the fact that most of the last advances in the knowledge of ammonia electrooxidation have been achieved applying differential electrochemical mass spectrometry (DEMS), as it is shown in the literature [5–7, 10, 15]. This technique allows the online detection of volatile and gaseous products formed during the electrochemical reactions, as well as the indirect characterization of the adsorbed species [20, 21], being in fact the most appropriate technique for this type of studies.

In the present paper, Pt–Ir bimetallic alloys were prepared following the electrochemical deposition method and characterized applying X-ray techniques, with the purpose to be used as electrodes for ammonia oxidation. This reaction was studied by cyclic voltammetry (CV), while DEMS allowed the detection of volatile products formed during the CV. Results for the alloy have been compared with those for Pt under the same experimental conditions. Pt–Ir electrodes were characterized again after

electrochemical oxidation of ammonia, and the changes in the structure, composition, and texture established.

Materials and methods

Pt–Ir alloys were prepared by electrodeposition from a pH= 2 sulfuric acid solution containing chloroplatinic acid and iridium chloride (atomic ratio 1:1), on a gold foil at 0.05 V_{RHE} and 60 °C during 30 min (otherwise indicated). The counter electrode was a platinum foil, and the reference electrode was a hydrogen electrode prepared in the electrolyte solution (reversible hydrogen electrode [RHE]). For DEMS, the Au electrode was sputtered onto the Teflon membrane used as the interface with the vacuum system (see later).

Ammonia solutions were prepared with ammonia sulfate in 0.1 M KOH, at different concentrations in the 2–50 mM range for CV and 5 mM for DEMS. Solutions were deoxygenated with purified Ar. All the experiments were performed at room temperature.

X-ray characterization of the alloys: X-ray diffractometry (XRD) patterns of the electrocatalysts were obtained with a Philips diffractometer, operating with CuK_α radiation (λ= 0.15406 nm) generated at 40 kV and 30 mA. Scans were done with a counting time of 5 s/step and 2θ values between 20 and 100°. Auger spectra were obtained with a SAM PHI 590A system, and the analysis was performed using 3 KeV and 2 mA. The surface was sputtered with Ar ions at 1 kV and 3 A min^{-1}. Spectra were acquired at different sputtering times and the peak amplitudes for Pt (168 and 1,967 eV), Ir (54 and 1,900 eV), and O (505 eV) followed. To determine the Pt–Ir atomic composition, Pt (1,967 eV), Ir (1,908 eV), and O (505 eV) were used (relative sensitive factors for these peaks were taken from Davis et al. [22]).

DEMS experiments: Mass spectrometric studies were performed in an electrochemical cell directly connected to a vacuum chamber containing the quadrupole mass spectrometer. The experimental setup allows the simultaneous detection of mass spectrometric cyclic voltammograms (MSCVs) for selected mass to charge ratios (m/z) and the CVs at a scan rate of v=0.01 V s^{-1}. The working electrodes were electrochemical-deposited Pt–Ir alloys and a porous Pt layer deposited onto a Teflon membrane that interfaces the electrochemical cell and the vacuum components. The real area of the electrodes was estimated from the CVs obtaining values of 11.2 and 2.1 cm^2 for Pt and Pt–Ir, respectively. For the latter, it has been considered that the charge involved in the hydrogen region is the same to Pt, as the alloy is the result of a 1:1 substitution, and hydrogen adsorption properties are similar for both metals. More details about the DEMS technique have been given elsewhere [20, 21].

Results and discussion

X-ray characterization of electrodeposited alloys

Figure 1a shows the XRD patterns of the electrodeposited Pt–Ir alloy on a gold foil before contacting the ammonia solution. Characteristic diffraction peaks of the face-centered cubic (fcc) Pt structure are observed, although shifted to higher 2θ values with respect to pure Pt. From this result, it is deduced the presence of a substitution alloy where the Pt atoms were replaced by Ir in the fcc structure of the former metal. On the other hand, from the calculation of the network crystalline parameters and assuming that the shift of these values with respect to that measured for pure Pt is directly proportional to the atomic percentage of the solute, a 70:30 atomic Pt/Ir composition is established.

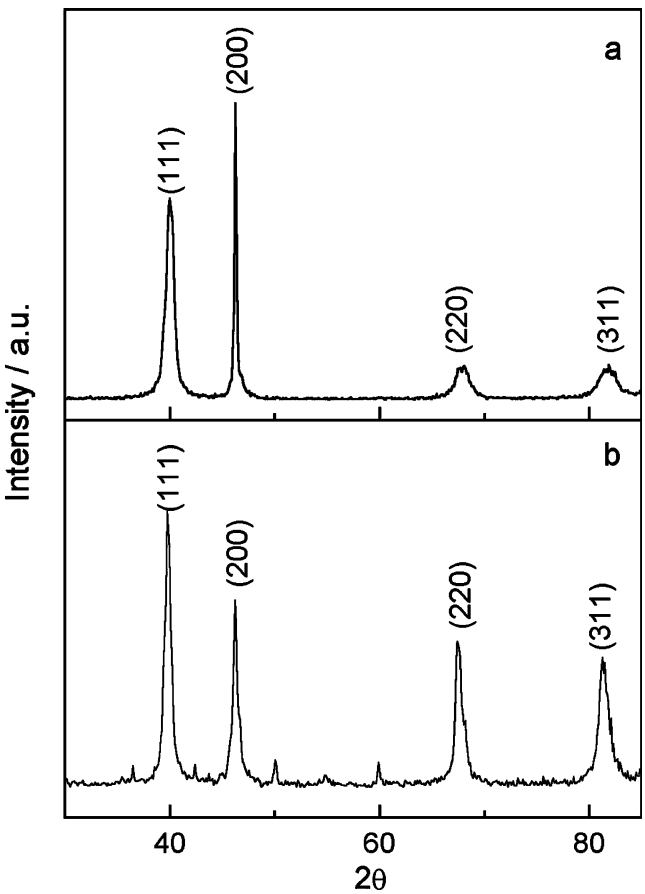

Fig. 1 XRD spectra for 60 min Pt–Ir electrodeposited alloy on a Au foil **a** before and **b** after using the catalysts for ammonia oxidation

The diffractogram in Fig. 1a displays preferential orientations indicating that the material has developed a crystallographic texture. The value of the texture coefficient (TC) was calculated by the inverse pole intensity technique [23] using the equation:

$$TC_{(hkl)} = \frac{I_{hkl}/I_{R(hkl)}}{\frac{1}{n}\sum_{i}^{n}\left(I_{hkl}/I_{R(hkl)}\right)_i} \quad (6)$$

where $I_{(hkl)}$ is the reflected intensity from (*hkl*) crystallographic planes in the textured specimen, $I_{R(hkl)}$ is the reflected intensity from (*hkl*) crystallographic planes from the random specimen, and n is the total number of reflections measured. TC for a particular set of planes (*hkl*) is proportional to the number of grains that are oriented with this plane parallel to the surface of the specimen. Powder of platinum was used as a random sample. TC<1 denotes that there are less than the random number of grains in a specific orientation, whereas TC>1 implies that the specimen has more than a random number of grains in that orientation. The evolution of TC values with the electrodeposition time for Pt–Ir alloys can be seen in Fig. 2. Similar textures are obtained in all cases with preference of planes (200) and (311).

The electrodeposit composition was also obtained from Auger spectra recorded at different sputtering times in the 20–530 eV range for the low-kinetic-energy region and in the 1,700–2,050 eV range for the high-energy-conversion region. Figure 3a displays the spectrum in the former region where peaks at 168, 54, and 505 eV are assigned to Pt, Ir, and O, respectively. In Fig. 3b, signals at 1,967 (Pt) and 1,900 eV (Ir) are observed. To determine the Pt–Ir atomic concentration, Pt (1,967 eV), Ir (1,908 eV), and O (505 eV) peaks were used. The alloy composition was evaluated applying the expression:

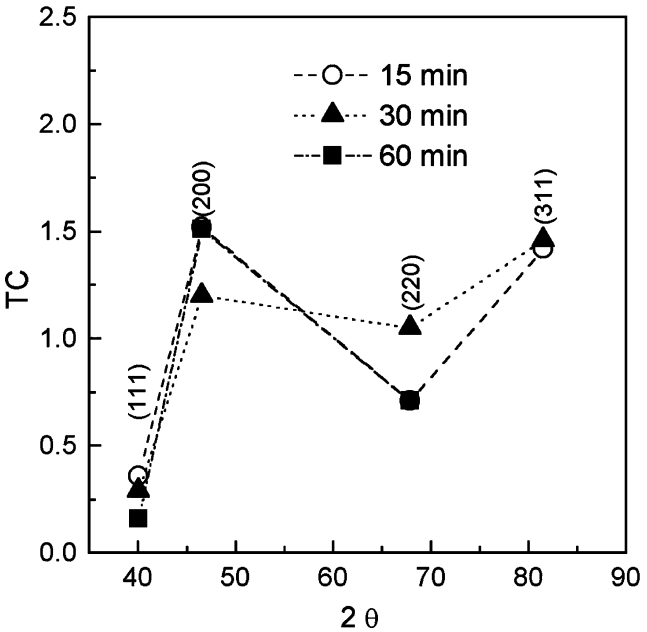

Fig. 2 Texture coefficient (TC) for Pt–Ir electrodeposits on Au calculated according to Eq. 6. Deposition times as indicated

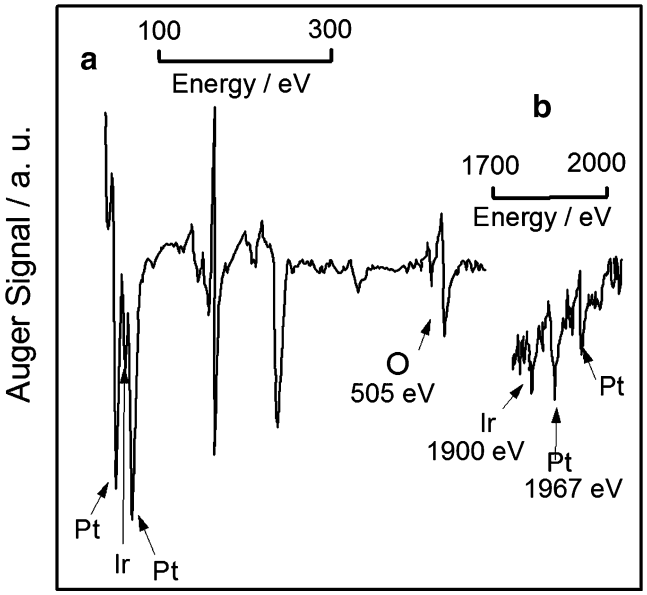

Fig. 3 Auger spectrum for Pt–Ir electrodeposits. Two spectral regions: **a** from 0 to 600 eV and **b** from 1,700 to 2,000 eV

$$Ni = \frac{Ii/Si}{Ii/Si + Ij/Sj + Ik/Sk} \quad (7)$$

where I are the peak intensities taken from Auger spectra (heights in arbitrary units) and i stands for Pt, j for Ir, and k for O. The sensitivity factors S are 0.02, 0.5, and 0.03 for Pt, O, and Ir at 3 keV [21].

Figure 4 shows the profiles for Pt, Ir, and O as function of the sputtering time. The Pt content slightly increases with the sputtering time, whereas that for Ir decreases. The amount of O is very low and decreases with the sputtering time. The average composition for the 60-min electrodeposited Pt–Ir alloy from the Auger analysis and that estimated from XRD parameter (70:30 for Pt/Ir) are in agreement.

Cyclic voltammetry

CVs for Pt-Ir (a) and Pt (b) electrodes recorded in 0.1 M KOH for different ammonia concentrations can be seen in Fig. 5. The onset for ammonia oxidation occurs in the region 0.40–0.50 V during the positive-going potential scan for both cases, but it is always positively shifted, at the same concentration, for Pt with respect to the alloy (see later, "DEMS studies"). In the range from 2 to 10 mM, the maximum current varies linear with the concentration.

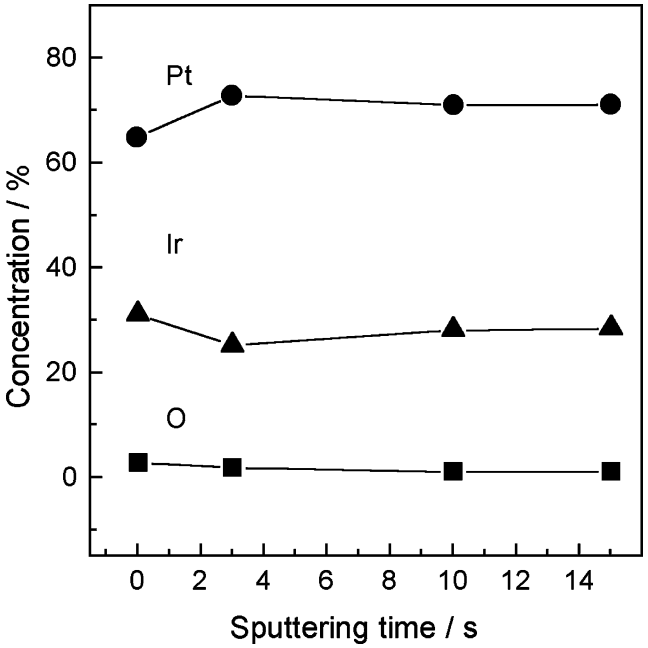

Fig. 4 Composition profile for Pt–Ir electodeposits calculated from Auger spectra according to Eq. 7

However, the potential position of this maximum shifts from 0.70 to 0.76 V in the case of Pt–Ir and from 0.66 to 0.90 V in the case of Pt. These results suggest the presence of a higher coverage of residues on the Pt surface, the amount of adspecies increasing with the concentration. The determination of the amount of these adsorbates present at the different potentials is in progress applying a flow cell procedure and will be reported in a forthcoming manuscript.

During the reverse scan, a cathodic current is apparent at $E<0.70$ V for both electrodes. This current could be related to the formation of reduction products or to the deprotonation of ammonia leading to adsorbed species. DEMS experiments permit to discern between both possibilities.

DEMS studies

CVs and MSCVs for Pt–Ir and Pt electrodes in a 5 mM ammonia solution prepared in 0.1 M KOH are given in Figs. 6 and 7, respectively. The upper potential limit was set at 1.0 V for the alloy to avoid differentiated dissolution of its components (in the case of Pt, the same potential limit was considered for the sake of comparison). Similar behavior is observed for Pt–Ir and Pt, with the production of N_2 (signal for $m/z=28$ corresponding to $[N_2]^+$), N_2O (ion current for $m/z=44$ assigned to the molecular ion $[N_2O]^+$), and other nitrogen oxides (signal for $m/z=30$, the fragment $[NO]^+$ from NO_x). However, some differences are remarkable.

For the Pt–Ir alloy (Fig. 6a), the onset for ammonia oxidation during the positive-going potential scan is observed at 0.48 V attaining a maximum in the current at 0.70 V. The shape of the CV coincides with the MSCV for N_2 production in this potential range (Fig. 6c), and therefore, 100% current efficiency to N_2 is deduced. However, a second increase in the faradaic current is detected at $E>0.90$ V, without response in this mass signal for $m/z=28$. Therefore, other oxidation products have to be formed. Accordingly, nitrogen oxides have been detected with an onset potential of 0.80 V: the ion current for $m/z=44$ associated to the production of N_2O (Fig. 6d) and the signal for $m/z=30$ assigned to the formation of all other nitrogen oxides different from N_2O (Fig. 6e). The maximum ion current is attained for both signals at the upper potential limit. During the negative potential sweep, an anodic current is observed in the CV for $E>0.80$ V (Fig. 6a) that can be related with the contribution of all these products whose signals progressively decrease from 1.00 to 0.80 V.

Results for the Pt–Ir alloy in Fig. 6 can be compared with those for Pt in Fig. 7. The electrochemical behavior is quite similar, but the following differences should be

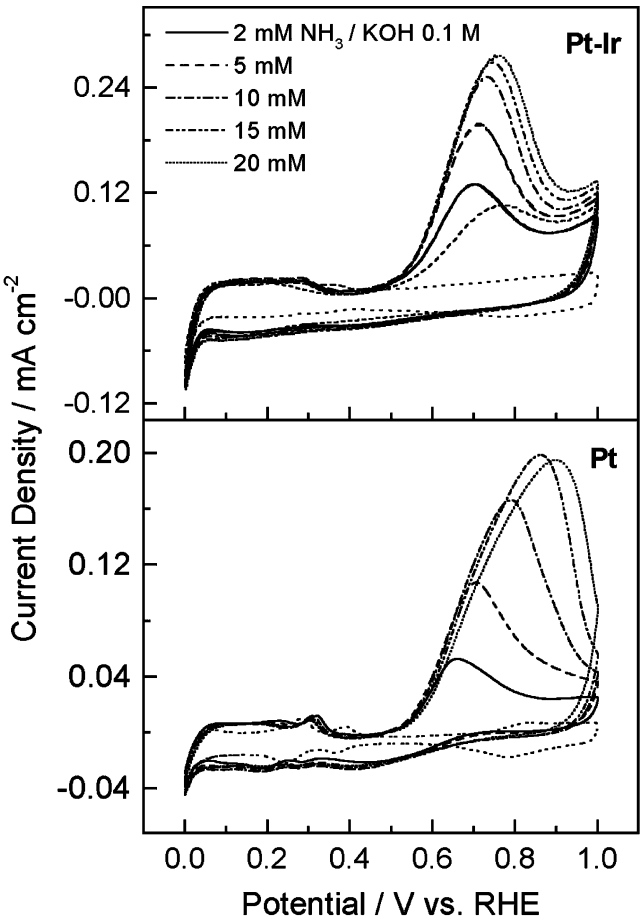

Fig. 5 CVs at different ammonia concentration as indicated for Pt–Ir and Pt electrodes. *Dashed line*: CV in 0.1 M KOH. $v=0.010$ V s^{-1}

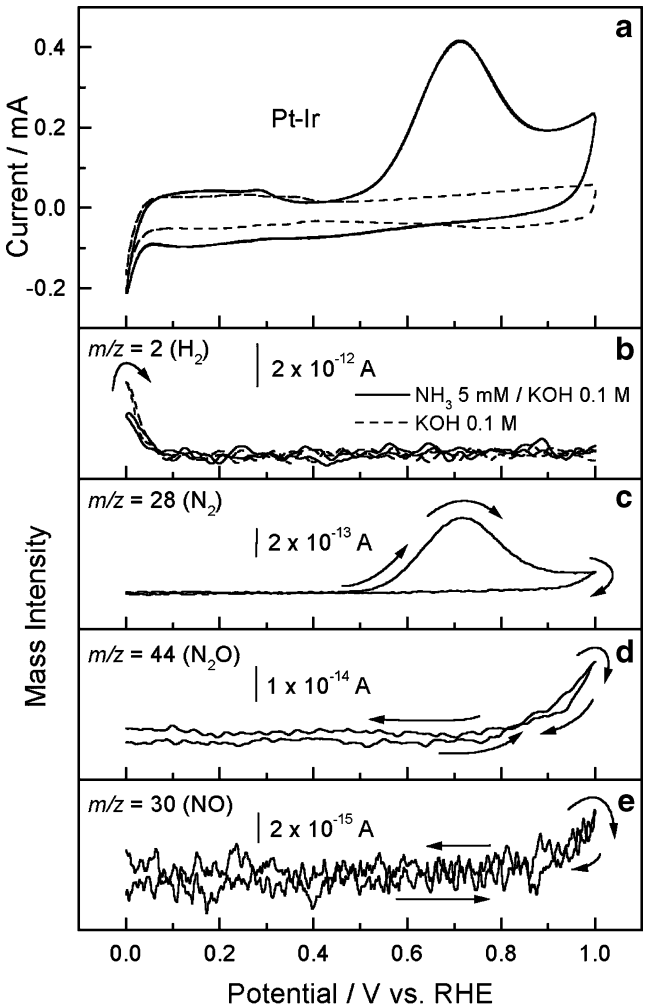

Fig. 6 CV (**a**) and MSCVs (**b**–**e**) during a DEMS experiment at Pt–Ir in 5 mM NH_3/0.1 M KOH. **b** m/z=2 (H_2); **c** m/z=28 (N_2); **d** m/z=44 (N_2O); and **e** m/z=30 (NO). *Dashed line*: CV in 0.1 M KOH. v= 0.010 V s^{-1}

addressed: (1) The onset potential for ammonia oxidation during the positive-going potential scan is slightly shifted to more positive potential (approx. 0.05 V), (2) the maximum in the production of nitrogen oxides is observed at 0.90 V during the positive-going potential scan, suggesting a faster production of these compounds at lower potentials than for Pt–Ir, and (3) higher amounts of the oxidation products are detected in the reverse scan, which are responsible for the higher anodic current in the CV for Pt (Fig. 7a).

From the integration of the MSCVs for m/z=28, 30, and 44, the yield of N_2 and nitrogen oxides can be also compared at both electrodes. The ratio of the ionic charges 28/(30+44) gives 217 and 267 for Pt and Pt–Ir, respectively, suggesting a higher selectivity toward N_2 for the alloy.

As already observed in Fig. 5, cathodic currents are apparent for Pt (Fig. 7a) and Pt–Ir (Fig. 6a) at E<0.70 V during the negative-going potential scan, especially for Pt in the 0.70–0.40 V potential range. No mass signals were recorded in this region, and consequently, the charge is proposed to be related with the deprotonation of ammonia through reactions 2 to 4 (see "Introduction"). In these reactions, adsorbed intermediates are formed on the surface as proved by the decrease in the amount of hydrogen produced at E<0.10 V (see Fig. 6b for the mass signal m/z=2 associated to $[H_2]^+$). The higher cathodic current observed for Pt confirms the previous trend in Fig. 5 concerning the higher poisoning of this electrode with respect to Pt–Ir.

The reduction of adsorbates to ammonia at E<0.40 V has been proposed by Wasmus et al. [5] from the detection of the mass signal for m/z=15 (because of fragmentation of ammonia) in this potential region for Pt black. This signal was not detected in our experiments, probably because of the lower specific surface area and different nature of our Pt electrode.

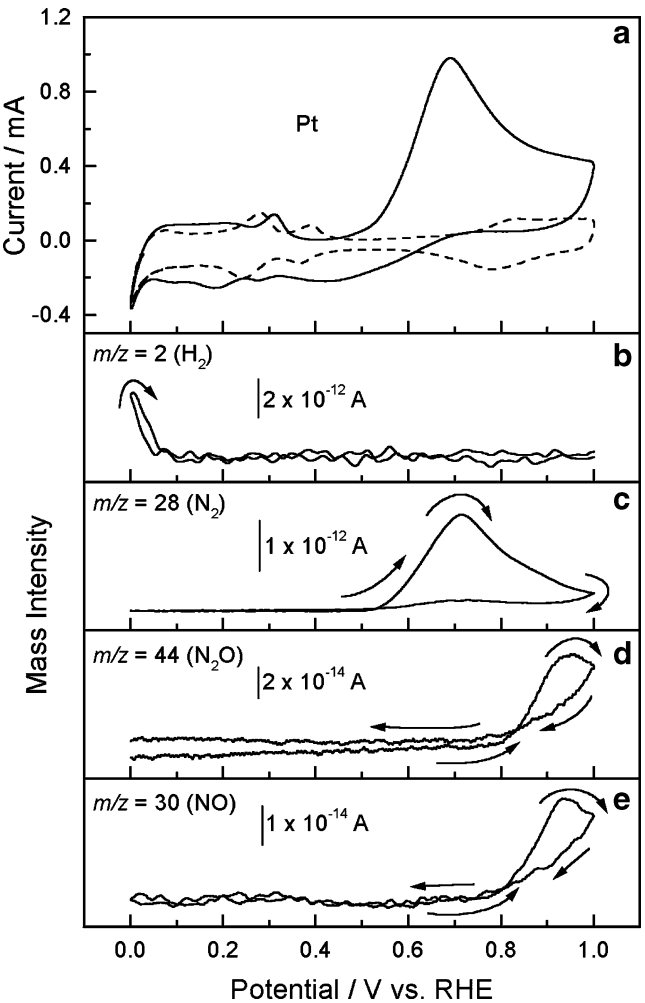

Fig. 7 CV (**a**) and MSCVs (**b**–**e**) during a DEMS experiment at Pt in 5 mM NH_3/0.1 M KOH. **b** m/z=2 (H_2); **c** m/z=28 (N_2); **d** m/z=44 (N_2O); and **e** m/z=30 (NO). *Dashed line*: CV in 0.1 M KOH. v= 0.010 V s^{-1}

X-ray characterization after ammonia oxidation

To study the stability of the electrodeposited alloy, XRD patterns were also obtained after using it as catalyst for ammonia oxidation during a 1-day experiment, about 10 h (Fig. 1b). The same composition was established for the alloy, but the patterns indicate a change in the sample texture. This change is confirmed from TC values calculated using Eq. 7): TC increases for planes (331) and (220) and diminishes for planes (200) and (111). From these differences, the trend for the variation is the following: (311)>(220)>(200)>(111). Then, it is established that ammonia oxidation induces changes on the surface of the catalysts with the development of certain planes in the crystallographic structure, favoring the less compact ones. In the same direction, it was proved that the highest activity toward ammonia oxidation at the basal Pt single is obtained at the (100) orientation and follows the trend (100)>(111) [8–9].

Conclusions

Pt–Ir alloys were prepared by the electrodeposition method and the activity toward ammonia oxidation studied. X-ray diffractograms revealed an fcc structure, resulting from the substitution of Pt atoms by Ir, with the development of a crystallographic texture. From XRD and Auger spectroscopy, a 70:30 atomic composition for Pt/Ir was established from 1:1 solutions. DEMS analysis has shown the selective production of N_2 in the 0.40–0.80 V potential region and the formation of nitrogen oxides for E >0.80 V. These results have been compared with Pt. The same oxidation products were detected, but the yield of N_2 is higher for the alloy, which also displays lower poisoning of the surface when increasing ammonia concentration. These results confirm Pt–Ir alloys as alternatives for Pt electrodes for technical applications as ammonia sensors or fuel cell materials. Further DEMS studies on the concentration effects on the product distributions for Pt–Ir alloys are in progress.

Acknowledgments Financial support from CONICET and CICYT-UNSE (Argentina) and MEC (MAT2005-0669-C03-02, Feder, Spain) is acknowledged. The authors wish to thank Dr. J. Ferron and Dr. R. Vidal from INTEC (Santa Fé, Argentina) for obtaining the Auger spectra. E. Moran acknowledges Universidad Nacional de Santiago del Estero (Argentina) and AECI (Spain) for financial support during the stay at the University of La Laguna.

References

1. Kordesch K, Gsellmann J, Cifrain M, Voss S, Hacker V, Aronson RR, Fabjan C, Hejze T, Daniel-Ivad J (1999) J Power Sources 80:190
2. Wojcik A, Middleton H, Damopoulos I, Van Herle J (2003) J Power Sources 118:342
3. Szpyrkowicz L, Kelsall GH, Kaul SN, De Faveri M (2001) Chem Eng Sci 56:1579
4. Szpyrkowicz L, Naumeczyk F, Zilio-Grandi F (1995) Wat Res 29:517
5. Wasmus S, Vasini EJ, Krausa M, Mishima HT, Vielstich W (1994) Electrochim Acta 39:395
6. Gootzen JFE, Wonders AW, Visscher W, van Santen RA, van Veen JAR (1998) Electrochim Acta 43:1851
7. López de Mishima BA, Lescano D, Molina Holgado T, Mishima HT (1998) Electrochim Acta 143:395
8. Vidal-Iglesias FJ, García-Aráez N, Montiel V, Feliu JM, Aldaz A (2003) Electrochem Commun 5:22
9. Vidal-Iglesias FJ, Solla-Gullón J, Feliu M, Baltruschat H, Aldaz A (2006) J Electroanal Chem 588:331
10. Ukropec R, Kuster BFM, Schouten JC, van Santen RA (1999) Appl Catal B 23:45
11. Gerischer H, Mauerer A (1970) J Electroanal Chem 25:421
12. II' chenko NI, Golodets GI, Avilova LM (1976) Kinet Catal 17:378
13. Papapolymerou G, Bontozoglou V (1997) J Mol Catal A 120:165
14. Van den Brock ACM, van Grondelle J, van Santen RA (1999) J Catal 185:297
15. de Vooys ACA, Koper MTM, van Santen RA, van Veen JAR (2001) J Electroanal Chem 506:1127
16. de Vooys ACA, Mrozek MF, Koper MTM, van Santen RA, van Veen JAR, Weaver MJ (2001) Electrochem Commun 506:1127
17. McKee DW, Scarpellino AJ, Danzig IF, Pak MS (1969) J Electrochem Soc 116:562
18. Endo K, Nakamura K, Katayama Y, Miura T (2004) Electrochim Acta 49:2503
19. Endo K, Katayama Y, Miura T (2005) Electrochim Acta 50:2181
20. Bittins-Cattaneo B, Cattaneo E, Konigshoven P, Vielstich W (1991) In: Bard AJ (ed) Electrochemical chemistry: a series of advances, vol. 17. Marcel Dekker, New York, p 181
21. Rodríguez JL, Souto RM, González S, Pastor E (1998) Electrochim Acta 44:1415
22. Davis LE, MacDonald NC, Palmberg PW, Riach GE, Weber RE (1976) Handbook of Auger electron spectroscopy. Physical Electronics, Eden Prairie, MN
23. Cullity BD (1967) In: Cullity BD, Stock SR (eds) Elements of X-ray diffraction. Addison-Wiley, Reading, MA (Chapter 14)